PHYSOR 2004 -The Physics of Fuel Cycles and Advanced Nuclear Systems: Global Developments
Chicago, Illinois, April 25-29, 2004, on CD-ROM, American Nuclear Society, Lagrange Park, IL. (2004)

Methods and Performance of a Three-Dimensional Whole-Core Transport Code DeCART

Han Gyu Joo[*1], Jin Young Cho[1], Kang Seog Kim[1], Chung Chan Lee[1] and Sung Quun Zee[1]
[1]*Korea Atomic Energy Research Institute, Yuseong, Daejeon, 305-600, Korea*

DeCART is a three-dimensional whole-core transport code capable of performing direct core calculations at power generating conditions without involving *a priori* homogenized few-group constant generation. In this paper, the methods of DeCART, which are characterized by the planar method of characteristics (MOC) solutions, the cell based coarse mesh finite difference (CMFD) formulation, the subgroup method for resonance treatment and subpin level thermal feedback, are presented as a whole. The performance of the code in the aspect of solution accuracy and computing speed is then examined using the applications to the C5G7MOX benchmark and its modified rodded variation problems and also to a three-dimensional core case involving thermal feedback. The examination indicates that accurate direct whole core calculations with subpin level thermal feedback for practical PWR problems are quite possible on affordable LINUX clusters within a time span of a few hours.

KEYWORDS: Whole-Core Transport, MOC, 2D-1D Coupling, CMFD, Subgroup Method, Subpin Level Thermal Feedback

1. Introduction

DeCART (Deterministic Core Analysis based on Ray Tracing) is a three-dimensional whole-core transport code capable of direct core calculation at power generating conditions. It does not involve *a priori* homogenized few-group constant generation. In order to deal with the heterogeneity at the pin cell level, the method of characteristic (MOC)[1] is used and the multigroup cross section data are obtained directly from a cross section library that is normally used in lattice transport codes. Various unique methods for three-dimensional (3-D) transport solution, resonance treatment, incorporation of pin-wise thermal feedback, and parallelization are employed in DeCART to cope with the huge computational problems.

Regarding the 3-D whole core transport solution, an effective approximate 3-D transport solution method involving two-dimensional (2-D)/one-dimensional (1-D) coupling through transverse leakages is employed. This approximate 3-D transport solution scheme was established because the straightforward application of the MOC to large 3-D core problems is prohibitive. The 2-D/1-D coupling scheme is realized within the framework of 3-D coarse mesh finite difference (CMFD) formulation which serves the dual functions of accelerating the 2-D radial MOC solutions [2,3] and incorporating the nodal expansion method (NEM)[4] based 1-D axial solution kernel. The diffusion approximation is applied to the axial solution by the NEM. The overall 3-D transport solution method is presented in the next section.

In DeCART, the neutron cross sections to be used in the multigroup transport calculation have to be provided for each isotope at each region to which different thermal conditions apply. The local temperature is thus reflected into the temperature dependence of the cross sections which includes the resonance broadening as well as the isotopic number density

[*] Corresponding author, Tel. +82-42-868-2651, FAX +82-42-868-8990, E-mail: joohan@kaeri.re.kr

changes, particularly in the moderator region. Other than the resonance cross sections, the incorporation of the temperature dependence of the cross section is achieved in a straightforward manner utilizing the temperature dependence data given in the cross section library. In order to determine the resonance cross section into which the spatial self shielding effect as well as the Doppler broadening should be properly incorporated, the subgroup method[5] is employed. The specific implementation of the subgroup method to deal with the nonuniform temperature distribution is presented in Section 3. The simultaneous solution of the neutron flux and temperature fields requires not only two independent solution modules, neutronic and thermal-hydraulic (T-H) solution modules, but also an iterative solution logic controlling the alternate execution of the two modules and the subsequent cross section update. The T-H solution module, which involves pinwise heat conduction calculation, and the overall feedback calculation logic are given in Section 4.

Although DeCART can eliminate the source of error associated with assembly homogenization and group condensation, it still has various other sources of error. The approximations involved in the 2-D/1-D coupled transport solution scheme and also in the temperature dependent subgroup method implementation are the primary sources of solution method errors. Another source of error lies in various multigroup cross section data. In order to evaluate the solution accuracy of DeCART, three-way verifications were performed. The first approach was to analyze known numerical and experimental benchmark problems. The 3-D C5G7MOX benchmark problem[6], its modified rodded variations and the VENUS-2 MOX critical core benchmark[7] were solved in this regard. In Section 5, details of the C5G7MOX analysis are given whereas as the VENUS-2 analysis result is given in a separate paper[8]. The second approach was to compare the DeCART solutions with those of a Monte Carlo code, MCCARD[9], which is capable of T-H feedback calculation. The consistent comparison with the MCCARD results is presented in a companion paper[10]. Only the DeCART execution performance for a 3-D minicore hot-full-power case is given in Section 5. The third approach was to compare with the results of the conventional two-step solution approach which had been proved successful in predicting the behavior of the operating commercial reactors. This comparison was given in a former paper[11] using the results of the HELIOS[5]/MASTER[12] lattice transport/nodal diffusion code system of KAERI.

Even though efficient solution methods were employed in DeCART, the direct 3-D whole core calculations with thermal feedback for the real power reactors pose yet a tremendous computational problem. The computational burden was resolved by employing parallel computing on affordable LINUX PC clusters. The parallelization and parallel performance were given in another former paper[13]. This paper provides only typical runtime performance of DeCART in Section 5 for the sake of demonstration. Section 6 concludes the paper.

2. 3-D Whole-Core Calculation Employing Planar MOC Solutions

Noting that most heterogeneity in a reactor problem appears in the radial direction rather than the axial direction, it is plausible to apply the MOC to resolve only the radial dependency and to use a lower order method for the axial dependency. In this regard, DeCART employs a planar MOC solution based 3-D CMFD formulation. Meshes of a pin cell size, i.e. ~1 cm, are used radially whereas meshes of 10 to 20 cm are used axially to reduce the number of planes. The MOC solution is used to generate dynamically homogenized cell cross sections and also the radial coupling coefficients at each plane. The axial dependency is resolved by the NEM during the solution of the 3-D CMFD problem. In the following the planar MOC solution based CMFD method is outlined with only essential details.

2.1 Decoupled Planar Transport Problem

Suppose a 3-D neutron transport problem involving several radial planes. As is normally done in the transverse-integrated method, the transport equation for a discretized angle *m* can be integrated over the axial direction on a plane (designated by plane index *k*) to yield:

$$\left(\varepsilon_m \frac{\partial}{\partial x} + \eta_m \frac{\partial}{\partial y}\right)\overline{\varphi}_m^k(x,y) + \Sigma_t^k(x,y)\overline{\varphi}_m^k(x,y) = \overline{Q}_m^k(x,y) - L_{z,k}^m(x,y) \quad (1)$$

where $\overline{\varphi}_m^k(x,y)$ is the axially averaged angular flux distribution and $\overline{Q}_m^k(x,y)$ is the axially averaged neutron source consisting of fission and scattering sources. $L_{z,k}^m(x,y)$ is the axial leakage representing the gradient of the axial angular flux distribution. This is defined as the difference between the angular fluxes at the top (T) and bottom (B) surfaces as follows:

$$L_{z,k}^m(x,y) = \frac{\mu_m}{h_k}\left(\varphi_m^{T,k}(x,y) - \varphi_m^{B,k}(x,y)\right). \quad (2)$$

As long as the axial leakage is obtained from the three-dimensional transport solution, the 2-D solution of Eq. (1) would reproduce the 3-D solution in the average manner. However, since this term cannot be determined in advance, approximations have to be introduced to this term to solve Eq. (1). In DeCART, the angular and spatial dependence of the axial transverse leakage is approximated using the axial diffusion solution which is determined from the CMFD problem. Specifically, the surface average net current and flux at the axial interface are used to represent the angular flux in the P1 form as follows:

$$\varphi_m^{T,k}(x,y) \approx \varphi_{m,k}^T = \frac{1}{2}\phi_k^T + \frac{3}{2}\mu_m J_z^{T,k} \quad (3)$$

Note that the radial dependency of the axial leakage within a cell is neglected here by using the cell average flux and current. Since Eq. (3) involves a polar angle dependency of the axial leakage, anisotropy should be introduced in the source term of the MOC equation.

2.2 Planar MOC Solution

Once the axial leakage sources are defined, the 2-D MOC problem can be established for each plane. The MOC solution in DeCART is obtained by employing a pin cell-based modular ray tracing scheme which is detailed in a former paper [14]. The ray tracing is performed for each group given the scattering, fission, and the axial leakage sources defined at each flat source region (FSR) by employing the following equation:

$$\varphi_{l,n}^{g,out} = \varphi_{l,n}^{g,in}\exp\left(-\frac{\Sigma_g s}{\sin\theta_l}\right) + \frac{q_{g,l}}{\Sigma_g}\left[1 - \exp\left(-\frac{\Sigma_g s}{\sin\theta_l}\right)\right] \quad (4)$$

where *l* and *n* are the polar and azimuthal angle indices, *s* is the length of the segment passing through a FSR by the ray designated by *l* and *n*, and $q_{g,l}$ is the source. The sources are assumed isotropic other than the axial leakage source which has polar angle dependence. The magnitude of the source term is determined by modulating the average magnitude determined for each cell by the CMFD calculation with the intra cell shape determined from the previous MOC solution step. For this, the scalar fluxes are stored at every FSR whereas the angular fluxes are stored only at the domain boundaries. Once the ray tracing is completed for each group, the scalar flux of each FSR and the current at each pin cell interface are updated. The scalar flux shape is used to determine the flux-volume averaged cross sections for the cell. The cell interface current is used to determine the current versus node average flux correlation which is needed in the CMFD formulation. At the reflective domain boundary, the outgoing angular fluxes are saved for use in the next ray tracing.

Since a tremendous amount of ray tracing calculations have to be performed with fine rays spacing and a large number of angular discretization in order to ensure solution accuracy,

efficient ray tracing calculation techniques including the usage of tabularized exponential functions and polar angle quadratures are employed in DeCART. For example, by using the four-polar angle quadrature set obtained by minimizing the error of the quadrature based value of the second Bickley function in the least square manner[15], DeCART achieves the similar solution accuracy to the eight equally spaced polar angle cases.

2.3 3-D CMFD Formulation

The radial MOC solutions provide the cell average cross sections and radial coupling relations which express the interface current as a function of the two adjacent node average fluxes. Since the details of the 2-D CMFD formulation is straight-forward as given in the former paper [2], only the axial coupling relation needed in the 3-D CMFD formulation is presented here. Using the NEM, the outgoing axial partial currents can be written in terms of the incoming partial currents, averaged flux, and moments as:

$$J_z^{+T,k} = T_1^k J_z^{-T,k} + T_2^k J_z^{-B,k} + T_3^k \bar{\phi}_k + T_4^k \tilde{\phi}_k^1 + T_5^k \tilde{\phi}_k^2 \tag{5}$$

where

$$T_1^k = \frac{1-960\beta_k^2}{(1+40\beta_k)(1+24\beta_k)},\quad T_2^k = \frac{-16\beta_k}{(1+40\beta_k)(1+24\beta_k)},\quad T_3^k = \frac{20\beta_k}{(1+40\beta_k)},$$

$$T_4^k = \frac{30\beta_k}{(1+24\beta_k)},\quad T_5^k = -\frac{70\beta_k}{(1+40\beta_k)}.$$

Here $J_z^{+T,k}$, $J_z^{-T,k}$ and $J_z^{-B,k}$ are partial currents, and $\bar{\phi}_k$, $\tilde{\phi}_k^1$ and $\tilde{\phi}_k^2$ are the average flux, the first and second flux moments. The ± superscripts designate the outgoing and incoming currents while the superscipt *T* and *B* indicate the top and bottom surfaces of Plane *k*. By replacing the outgoing partial current appearing in the 3-D CMFD equation with that given in Eq. (5), the nodal balance equation at Node (*n*,*k*) can be expressed in terms of node average fluxes, incoming partial currents and the axial flux moments as:

$$\begin{aligned} -\frac{1}{h}\sum_{j=1}^{N_{rad}^{n,neig}} \left(\tilde{D}_j^{n,k} + \hat{D}_j^{n,k}\right)\bar{\phi}^{j,k} + \left\{\Sigma_a^n + \frac{2T_3^k}{h_z^k} + \frac{1}{h}\sum_{j=1}^{N_{rad}^{n,neig}} \left(\tilde{D}_j^{n,k} - \hat{D}_j^{n,k}\right)\right\}\bar{\phi}^{n,k} \\ = \bar{S}^{n,k} - \frac{1}{h_z^k}\left(T_1^k + T_2^k - 1\right)\left(J_z^{-T,k} + J_z^{-B,k}\right) - \frac{2T_5^k}{h_z^k}\tilde{\phi}_2^n \end{aligned} \tag{6}$$

where $N_{rad}^{n,neig}$ is the number of radial neighboring nodes of Node *n* and $\bar{S}^{n,k}$ is the source including fission and scattering. The incoming currents and the second moments appearing on the right hand side are assumed to be available from the previous iteration step. Eq. (6) is formed for each plane and each group. The one-group planar problem is solved by a Krylov subspace method employing the blockwise incomplete LU factorization preconditioner[16] which has a good convergence characteristics even with a small radial mesh size amounting to a pin cell. For each plane, the groupwise calculation is performed with the scattering source updated. After a few group sweeps, the axial boundary condition involving incoming currents and the moments is updated. After the completion of the planar sweep, one outer iteration step is completed and the eigenvalue and the fission sources are updated accordingly. Since Eq. (6) is a planar problem in which the axial coupling term is specified as the boundary condition, the planar CMFD problems can be solved in parallel in the block Jacobi manner.

3. Resonance Treatment by Subgroup Method for Nonuniform Temperature Conditions

In order to determine self-shielded resonance cross sections for the given configuration and

temperature condition, the subgroup method realized in the HELIOS code [5] is employed in DeCART with a correction to incorporate the nonuniform temperature distribution. The basic idea of the subgroup method is to approximate the continuous variation of the resonance cross section with a set of stair-like variation within a coarse energy group containing the resonance. In the following the implementation of the subgroup method is presented briefly for the basic uniform temperature case and then for the nonuniform temperature case.

3.1 Basic Subgroup Method Implementation

With the subgroup method, the effective cross section for a resonance energy group at a small flat source region (FSR) in which the local temperature *T* is given is represented by:

$$\bar{\sigma}(\mathbf{r},T)=\frac{\sum_i w_i(T)\phi_i(\mathbf{r},T)\sigma_i}{\sum_i w_i(T)\phi_i(\mathbf{r},T)} \tag{7}$$

where σ_i is the *i*-th subgroup level (or the height of the *i*-th stair), $\phi_i(\mathbf{r},T)$ and $w_i(T)$ are the subgroup flux and the subgroup weight, respectively, which depend on the local temperature. In the HELIOS subgroup method, the subgroup flux is determined as a function of the equivalence cross section which forces the equivalence between the heterogeneous flux obtained for the actual geometry and the homogenous flux determined with a virtual background cross section. In order to determine the heterogeneous flux at each region in a *uniform temperature condition*, the following subgroup fixed source problem (SGFSP), which is a one-group neutron transport problem, is to be solved:

$$\Omega\bullet\nabla\varphi(\mathbf{r},\Omega)+\left(N_R(\mathbf{r})\sigma_m+\lambda\Sigma_p(\mathbf{r})\right)\varphi(\mathbf{r},\Omega)=\frac{1}{4\pi}\lambda\Sigma_p(\mathbf{r}) \tag{8}$$

where σ_m is a prespecified *m*-th subgroup level, N_R is the number density of the resonance isotope of interest, λ and Σ_p are the intermediate resonance parameter and the macroscopic potential cross section, respectively. This equation is formed based on the observation that the neutrons belonging to a subgroup would experience the same absorption cross section regardless of the position and also based on the assumption that the flux above the resonance energy group is independent of the position and the magnitude is unity. Thus no flux dependent expression appears on the right hand side. Once the transport solution of Eq. (8) is obtained, the scalar flux, which is called the heterogeneous flux, is used to determine the equivalence cross section at each FSR using the following enforced equivalence relation:

$$\phi_m^{het}=\frac{\lambda\Sigma_p+\Sigma_e^m}{N_R\sigma_m+\lambda\Sigma_p+\Sigma_e^m}\Rightarrow\Sigma_e^m=\frac{\phi_m^{het}}{1-\phi_m^{het}}N_R\sigma_m-\lambda\Sigma_p\,. \tag{9}$$

The equivalence cross section is functionalized on the prespecified subgroup level after solving multiple SGFSPs with a different prescribed subgroup level each time. The equivalence cross section determined from this function is later used to determine the flux for each subgroup level for use in Eq. (7).

3.2 Consideration of Temperature Dependence

The above scheme can be applied to uniform temperature cases without any significant problem other than the problem associated with the flat flux assumption for the energy groups above the resonance. In case of the nonuniform temperature condition, however, a major modification has to be introduced in the formulation of the SGFSP problem. Suppose that the resonance group is divided into sufficiently many subgroups so that there are fine-width stairs formed. A neutron belonging to a subgroup close to the resonance peak at an FSR of temperature T_L is now transported to an adjacent region of temperature T_H. If $T_H>T_L$, the

neutron would experience a lower cross section due to Doppler broadening. In this regard, Eq. (8) can not be formed with the constant subgroup level for the nonuniform temperature case.

Under the concept of the subgroup method in which the temperature dependence is represented by the subgroup width (or weight) rather than by the subgroup level, it is not straightforward to incorporate the temperature dependence of the resonance cross section. As an approximate solution to this problem, a forced subgroup level adjustment scheme is employed in DeCART. This scheme is to use the relative value of the temperature dependent widths to determine the proper subgroup level.

Consider two regions having different temperatures and also the widths of the two subgroups levels. One is a high level subgroup whose height is close to the resonance peak and the other is a low level subgroup whose height is much lower than the average level. The width of the high level subgroup at the higher temperature region would be narrower than the corresponding subgroup width at the other region because of the broadening. Conversely, the width of the low level subgroup would be wider at the high temperature region. Based on this observation, it is plausible to adjust the cross section to be used in the SGFSP such that it is proportional to the subgroup width. The proportional constant can be taken from a reference temperature condition. The core average fuel temperature can be used as the reference temperature. The ratio of the *m*-th subgroup level to the subgroup width for the average temperature can be taken as the proportional constant. Namely, σ_m in Eq. (8) is replaced by the following:

$$\sigma_m(T(\mathbf{r})) = \frac{w_m(T(\mathbf{r}))}{w_m(T_{avg})}\sigma_m \,. \tag{10}$$

Note that Eq. (8) is retrieved for the uniform temperature condition even when the cross section adjustment scheme of Eq. (10) is used.

Once the solution to the SGFSP formulated with temperature dependent subgroup levels is obtained, the equivalence cross section can be determined in the same way as the basic case of Eq. (9), but again σ_m replaced by Eq. (10). The resulting equivalence cross section is in turn functionalized by taking the adjusted prescribed cross section level of Eq. (10) as the independent variable. When the effective cross section is calculated by Eq. (7), the flux for the *i*-th subgroup level is determined by the following equation incorporating the temperature dependent adjustment of the subgroup level:

$$\phi_i(T) = \frac{\lambda\Sigma_p + \Sigma_e^i(T)}{N_R\alpha_i(T)\sigma_i + \lambda\Sigma_p + \Sigma_e^i(T)} \;;\; \Sigma_e^i(T) = f\left(\alpha_i(T)\sigma_i\right) \;;\; \alpha_i(T) = \frac{w_i(T)}{w_i(T_{avg})} \,. \tag{11}$$

The modified subgroup method implementation described above requires the temperature distribution to be known before the SGFSP calculation. Since the temperature distribution is one of the solutions to be determined along with the flux distribution which depends on the resonance cross sections, the SGFSP in principle has to be performed several times with the updated temperature distribution each time. This would be too costly though because the SGFSP is itself an expensive transport problem. Thus the SGFSPs are solved only once in DeCART after a partially converged solution is obtained to generate a good approximation to the temperature distribution.

4. Incorporation of Subpin Level Thermal Feedback

In order to incorporate the thermal feedback effect into the flux calculation, both the Doppler and coolant number density effects should be properly taken into account in the calculation of the regional multigroup macroscopic cross sections. In DeCART, uniform cross section regions (UXR) are defined within each pin cell. Specifically, a group of concentric

regions are defined as the UXRs within the pellet and cladding while only one UXR is defined for the entire coolant region of the pin channel. Thus the fuel temperature distribution and the coolant temperature and density must be obtained to determine the temperature dependent cross sections. In order to obtain the temperature field, a simplified one-dimensional heat transfer solver applicable to closed pin-wise channels is used. The radial heat conduction solution is obtained by the finite difference method that involves several meshes in the pin. The resulting fuel temperature distribution is used to update the resonance cross sections as described above. The bulk coolant density is used to update the hydrogen and oxygen number densities. Since the heat conduction rings do not have to coincide with the flat source rings used for the MOC calculation, a mapping scheme is employed to obtain the volume average temperature for each flat source region. Typically, six equispaced conduction rings are used inside the pellet whereas three equivolume rings which are further divided azimuthally to eight slices are used as flat source regions.

In order to obtain converged flux and temperature fields which are coupled with each other, an iterative solution scheme involving alternate neutronics and T-H calculations need to be implemented. In the DeCART's CMFD framework, the T-H calculation is performed right after the CMFD calculation. The new T-H condition is used to determine the temperature dependent regional cross sections for use in the subsequent MOC calculation. The temperature dependence of the regional cross section is reflected into the CMFD calculation via the cell homogenization process performed after the MOC calculation. The radial cell coupling coefficients are updated as well for the subsequent CMFD calculation. The overall calculation flow is depicted in Fig. 1.

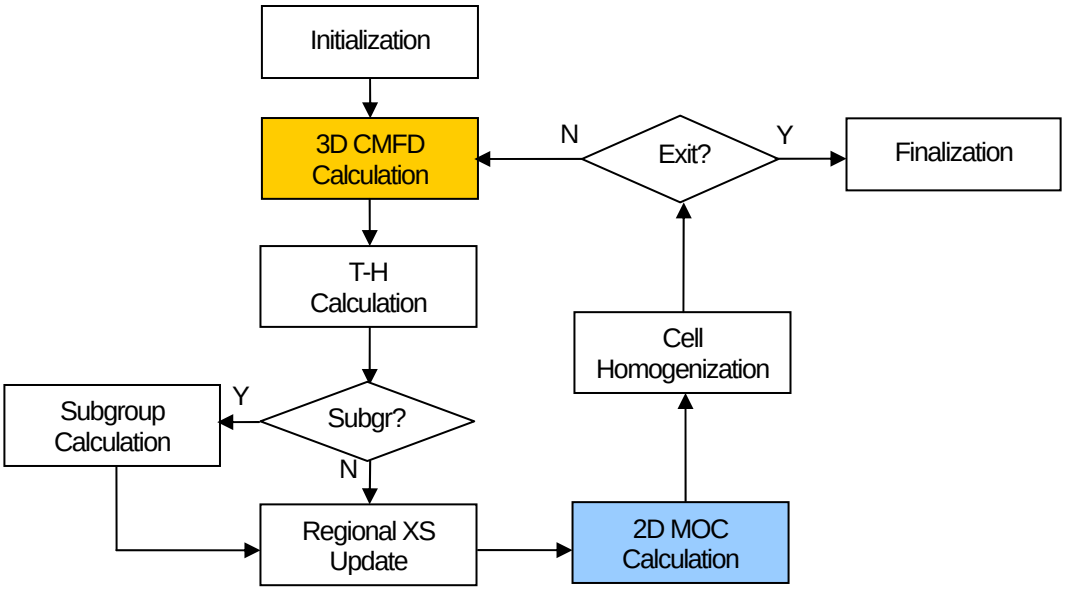

Fig. 1 DeCART Calculation Flow

5. Performance Examination

The performance of a reactor code analysis code can be characterized by both the solution accuracy and the computing speed. Regarding the solution accuracy of DeCART, three-way verifications had been performed as stated in the introduction. The analysis of the C5G7MOX and its modified rodded variations are detailed in the following subsection. This is to verify the 3-D transport solution method of DeCART given the multigroup cross sections. The

analysis results for the VENUS2 critical core benchmark are not repeated here by stating only that the k-effective for the 3-D problem is 0.99724 and the maximum C/E value is about 1.08. This result proves that the cross section library and the transport solution module of DeCART are sound. The most extensive verification was carried out by the consistent comparison with the results of the MCCARD Monte Carlo code for cases without and with T-H feedback on various geometries. Since the companion paper details the comparison, only the computing performance in the aspect of convergence characteristics and the computing time are given in the second subsection for a realistic 3-D core problem involving T-H feedback.

5.1 C5G7 MOX Benchmark and Its Rodded Variation Problems

In order to examine the accuracy of the DeCART 3-D transport solution method, the C5G7MOX benchmark problem set was solved first. This problem set consists of a 2-D and a 3-D problem. The core is loaded with sixteen UOX and MOX fuel assemblies arranged as shown in Fig. 2 for the upper right quadrant. Seven-group cross sections are provided and the reference solutions are available from the MCNP calculations involving 300 million histories. The DeCART calculation for this problem set was performed with a fine ray tracing parameters, namely, 0.2 mm ray spacing, 16 azimuthal angles per 180 degrees and 4 polar angles for 90 degrees. For the 3-D problem, the active core was divided into 10 planes (9x20 cm + 1x12.78 cm) and 2 additional planes were added to the top reflector (10 cm and 11.42 cm thick, respectively). Table 1 shows the eigenvalue and maximum and RMS power distribution errors while Fig. 3 shows the pin power errors for the 3-D problem. As shown in the table, the eigenvalue error is 6 pcm and the maximum pin power error is less than 2%. This demonstrates the excellent accuracy of the DeCART transport solver. On the other hand, the computing time for the 2-D case was 13 minutes on a 2.4 GHz Pentium IV Linux machine. For the 3-D case, the computing time of a parallel execution with twelve 2.4 GHz CPUs on a LINUX cluster was 30 minutes.

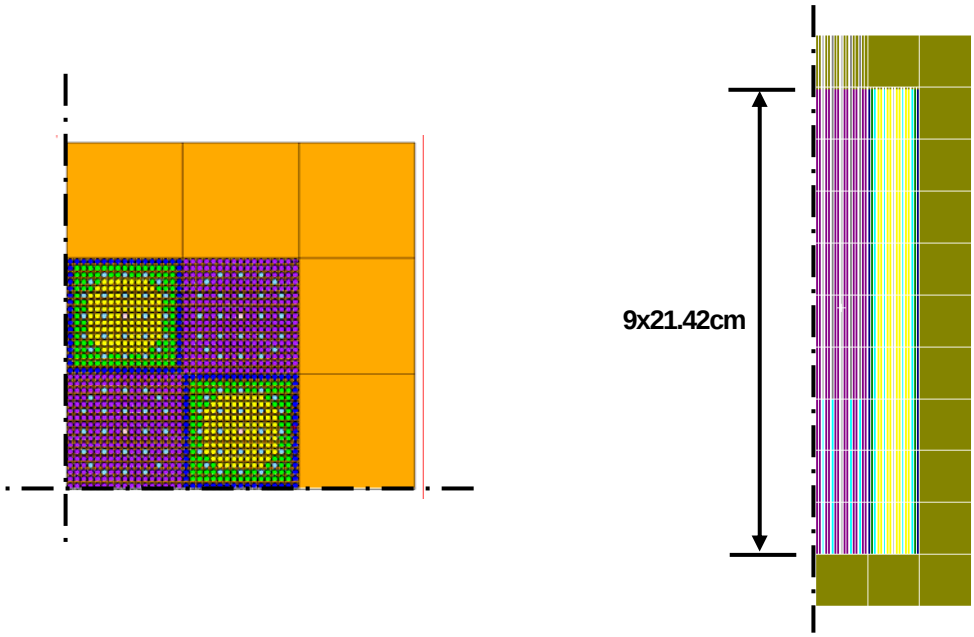

Fig. 2 Configurations of Modified Rodded Variations of C5G7MOX Benchmark Problem

Table 1 Results Summary for C5G7MOX Benchmark Problems

Cases	Eigenvalue		Eigenvalue Error, pcm	Pin Power Error, %	
	Reference	DeCART		Max.	RMS
2-D	1.18655	1.18663	6	1.80	0.46
3-D	1.18381	1.18389	6	1.89	0.50

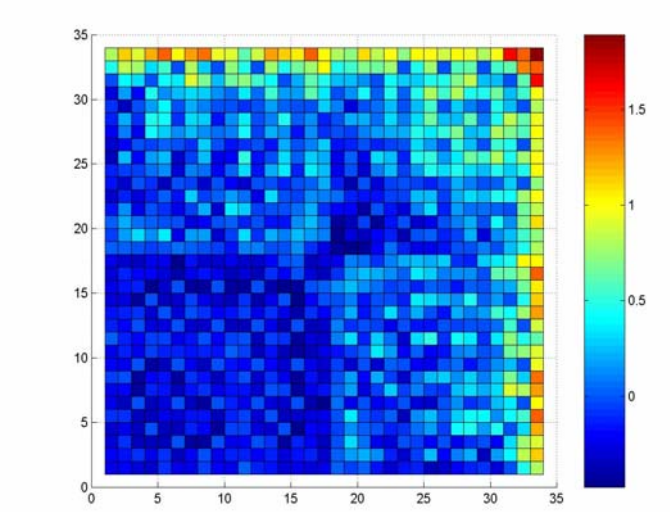

Fig. 3 DeCART Relative Pin Power Error (%) for the 3-D C5G7MOX Problem

This benchmark problem is, however, not adequate to the examination of the 3-D solution method because it does not involve any severe axial variation of materials. Although there are original rodded variation problems newly issued, different rodded variation problems are examined here in order to introduce more severely distorted axial power shapes. In the modified rodded problems, the axial configuration of the problem is changed such that both axial boundaries are vacuum instead of the reflective symmetry at the bottom in the original problem. The bottom reflector which has the same composition and dimension as the top reflector is added as shown in Fig 2. There are nine fuel planes defined in the core whose thickness is 21.42 cm. In the first problem, the central UOX assembly is rodded upto 4 planes (Case R4) with the same rod cross sections as the original rodded variation problems and the other is rodded upto 6 planes (Case R6). Note that the top reflector is rodded as well.

For the rodded problems, eleven equal thickness (21.42 cm, nine in the active core and two in the axial reflectors) planes were used in the base DeCART model. Other models with thinner plane thicknesses (or thinner axial node sizes) were also performed to examine the solution sensitivity on the axial node size. Three models involving 22, 44, and 88 plane models, which consist of 10.71, 5.335, and 2.6775 cm axial nodes, respectively, were used. The reference solutions for these two problems were obtained from the MCNP calculations involving 200 million histories. In Fig. 4, the axial power shapes are compared for the two rodded cases and the planar radial power shapes are shown in Fig. 5 for the two planes in the six plane rodded case. As shown here, the six plane rodded case involves a more highly bottom skewed power shape and thus is a more difficult problem. As a result, larger errors are noted for the six plane rodded case as indicated by the error information given in Fig. 4 and Table 2.

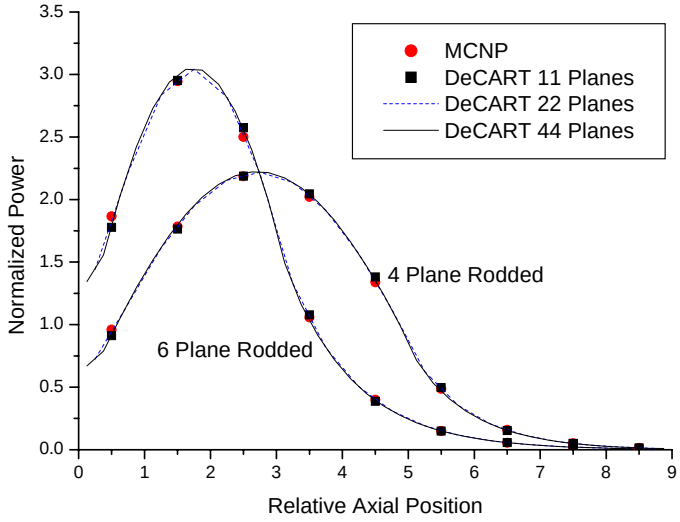

Fig. 4 Axial Power Shapes of the Modified Rodded Variation Problems

Although the DeCART axial power shapes for eleven plane cases look similar to those of the MCNP cases, the detailed 3-D power distribution exhibits nontrivial errors as indicated in Table 2. The maximum local power error is greater than 12% for the six plane rodded case and the RMS error is about 5%. This error can be reduced significantly if the plane thickness is halved. The twenty-two plane case has 1.9% RMS error and 3.4% maximum local power error. Further reduction of the plane thickness can improve the solution, but only marginally as shown in Table 2 as well as in Fig. 6 which shows the planar RMS errors. It is shown in the table and figure that the DeCART solution indeed converges as the plane thickness decreases. However, there are finite errors in the eigenvalue and power distribution which would result from the diffusion approximation used in the axial solution. Yet, the eigenvalue error for the severely rodded case is less than 90 pcm and the maximum local power error is less than 4%. This analysis indicates that a plane size of about 10cm is enough for DeCART calculations even for rodded cases and the DeCART 3-D transport solution scheme characterized by the 2-D MOC/1-D NEM coupling works fine.

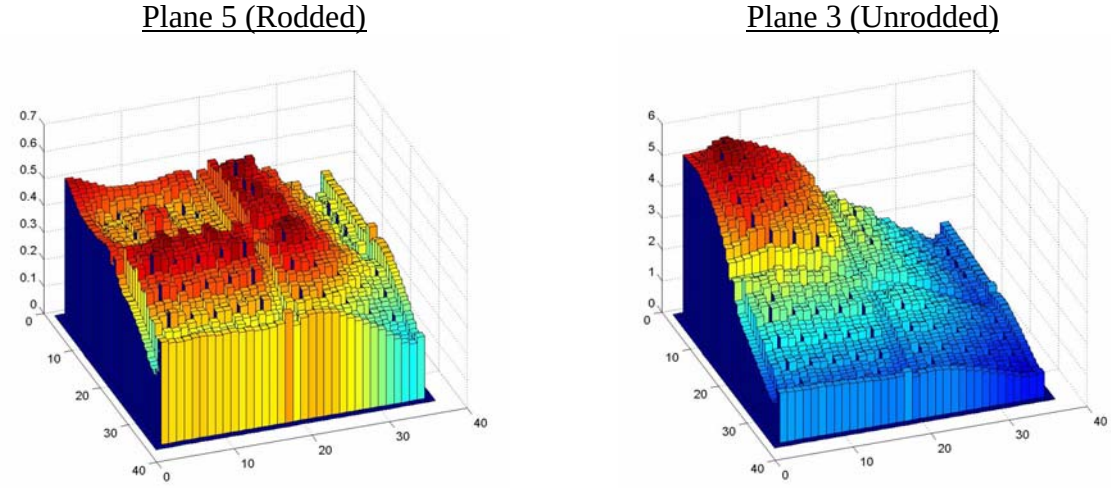

Fig. 5. Planar Radial Power Shape for 6 Plane Rodded Case (Planes 4 through 9 Rodded)

Table 2 Result Summary for Rodded Cases

Number of Planes	Plane Thickness cm	Eigenvalue Error, pcm		3-D Pin Power RMS Error, %		Maximum Absolute 3-D Pin Power Error		Maximum Relative 3-D Pin Power Error, %	
		R4	R6	R4	R6	R4	R6	R4	R6
11	21.42	-1.5	-25.7	2.95	4.68	0.140	0.229	6.67	12.12
22	10.71	-20.8	-76.4	0.97	1.87	0.061	0.118	3.71	3.39
44	5.355	-23.7	-82.7	0.84	1.68	0.049	0.100	3.84	3.74
88	2.6775	-23.7	-81.9	0.84	1.67	0.048	0.099	3.80	3.79

* R4, R6 are for the four and six plane rodded cases, respectively; Reference Eigenvalues: 1.16139 and 1.13277 for R4 and R6, respectively.

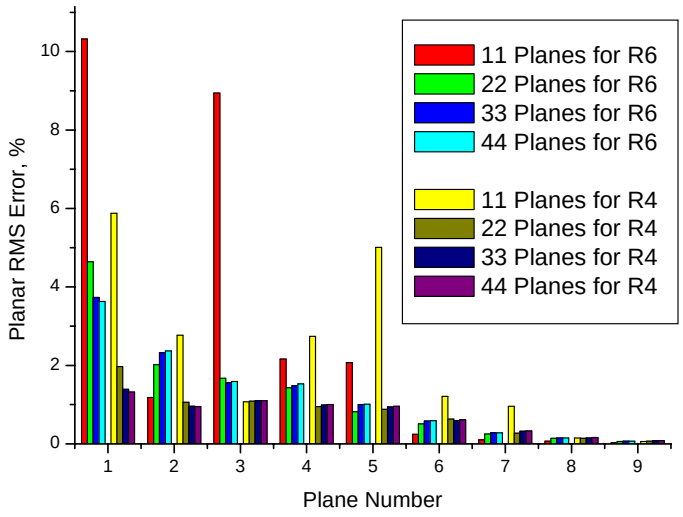

Fig. 6 Planar Absolute RMS Error for Rodded Cases

5.2 Computational Performance for a 3-D Core with T-H Feedback

The last problem defined in the test problem set given in the companion paper[10] is a 3-D minicore problem at hot-full-power condition (HFP). This minicore consists of five rows of reduced height (2 meters) typical 17x17 fuel assemblies and is reflected with water. To solve this problem, all the calculation modules of DeCART, namely, the cross section manipulation module, the subgroup fixed source calculation module, the 3-D transport solution module, and the T-H calculation modules are used. Fig. 7 shows the radial pin power and fuel temperature distribution obtained for this problem. As presented in the other paper, the k-effective error of the DeCART solution is about 260 pcm and the maximum pin power error is about 3.7%. This proves a good agreement with the Monte Carlo solutions obtained with thermal feedback.

The convergence of the relative residual which is an indicator of the imbalance of the neutron production and loss obtained for the DeCART calculation for this case is shown in Fig. 8 along with the convergence of the core k-effective and the maximum centerline fuel temperature. The abrupt jumps noted in the residual convergence behavior are due to the MOC updates which modify the cell homogenized cross sections and the coupling coefficients. In-between the jumps, only the multigroup CMFD calculations are performed. It is noted that the k-effective converges after only three MOC calculations.

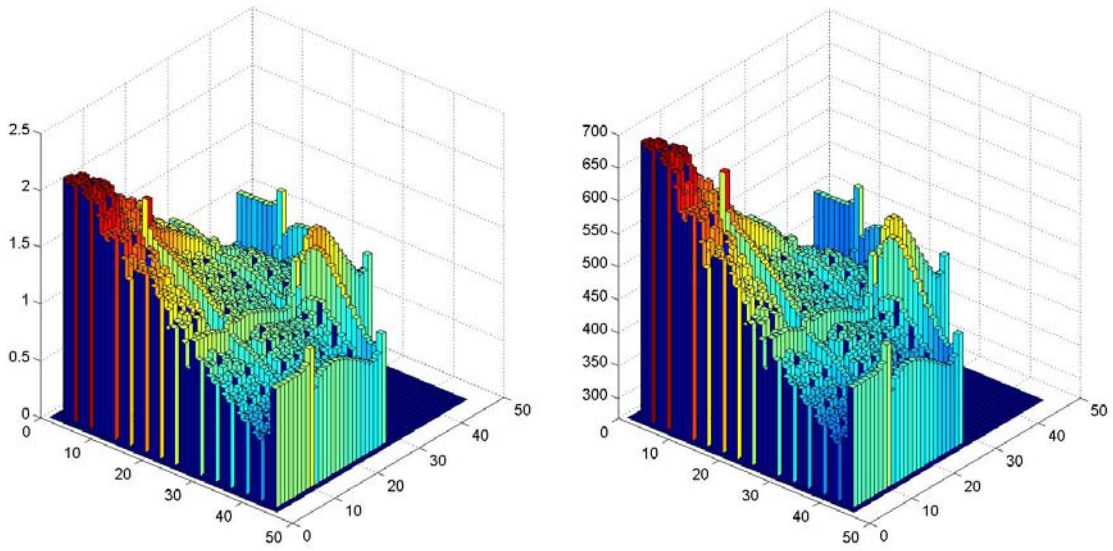

Fig. 7 Pinwise Radial Power and Fuel Temp. (°C) Distributions for HFP Minicore Problem

The first centerline fuel temperature point shown in Fig. 8 was obtained from the power distribution determined by the first CMFD calculation. Thus no MOC calculation is performed at this time. However, the centerline fuel temperature of 1360°C at this point is not quite far from the converged value of 1410°C. The temperature and density distribution corresponding to this first point is used in the subgroup fixed source calculation. Therefore it can be surmised that the temperature dependent subgroup calculation performed before the first MOC calculation would be reasonably accurate.

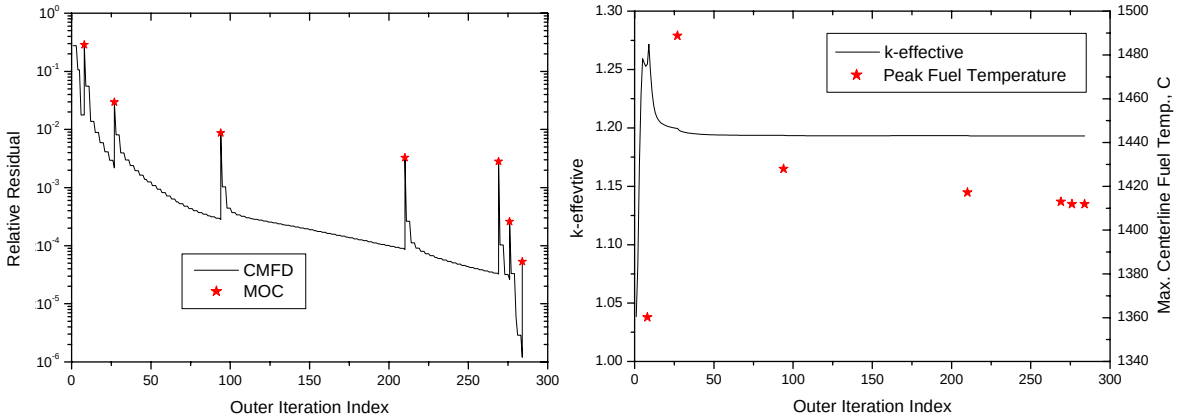

Fig. 8 Convergence Behavior for the HFP Minicore Problem

The computing times spent by the primary modules of DeCART for the minicore problem are shown in Table 3. This case was performed on a LINUX cluster with twenty-four 1.8 GHz Pentium-IV CPUs. The total run time of about 90 minutes for this forty-five group pin-by-pin transport calculation is not considered prohibitive. It is expected that routine direct whole core calculations for design analyses are quite possible in near future. In the aspect of parallel computing, the communication time fraction of 46% seems to overkill the parallel efficiency. But the large communication time which is spread over the various solution modules is unavoidable on a distributed memory machine and in a situation involving fine-grain

parallelism, particularly needed for the CMFD solution. The advantage of using distributed machines is though that they are affordable and large problems requiring excessive memories can be solved on those machines.

Table 3 Computing Time Breakup for the HFP Minicore Problem (24 CPUs)

Module	Time, sec	Fraction, %
Sub Group Calculation	794	14.7
CMFD	1229	22.8
Ray Tracing (MOC)	2794	51.9
Cross Section, T/H etc.	572	10.6
Communication	2489	46.2
Total	5389	

6. Conclusion

The capability of the direct 3-D whole core transport calculation with subpin level thermal feedback was realized in the DeCART code employing the planar MOC solution based CMFD formulation and the subgroup method. Although the direct core calculation is computationally very demanding, the solution can be obtained in a practical time span (less than a few hours) on affordable LINUX platforms through the use of the efficient solution methods and parallel processing. The 2-D MOC/1-D NEM coupled 3-D CMFD solution scheme which is one of the key components delivering the solution efficiency was proven to be sufficiently accurate through the examinations of the modified rodded variation problems of the C5G7MOX benchmark. Although it was shown that quite accurate solutions are obtainable for the 3-D cases with thermal feedback through the comparison with the corresponding Monte Carlo solutions, the eigenvalue error of about 260 pcms and the maximum pin power error of about 3% suggest further improvements. In this regard, the investigation of the temperature dependent implementation of the subgroup method and the isotropic scattering treatment is underway.

Acknowledgements

This work was supported by the International Nuclear Energy Research Initiative (I-NERI) program jointly funded by the Ministry of Science and Technology of Korea and the Department of Energy of the United States.

References

1) M. J. Halsall, “CACTUS, A Characteristics Solution to the Neutron Transport Equations in Complicated Geometries,” AEEW-R-1291, United Kingdom Atomic Energy Authority, Winfrith (1980).
2) H. G. Joo, et al., “Dynamic Implementation of the Equivalence Theory in the Heterogeneous Whole Core Transport Calculation,” *PHYSOR2002*, Oct. 7-10, 2002, Seoul, Korea, Paper 13A-02, CD-ROM (2002).
3) K. Smith and J. D. Rhodes, III, “Full-Core, 2-D, LWR Core Calculations with CASMO-4E,” *PHYSOR2002*, Oct. 7-10, 2002, Seoul, Korea, Paper 13A-04, CD-ROM (2002).
4) H. Finnemann, et al., “Interface Nodal Current Techniques for Multidimensional Reactor Calculations,” Atomkernenergie, **30**, 123 (1977).

5) R. J. J. Stamm'ler, "HELIOS Methods," Studsvik Scanpower (2002).
6) OECD/NEA, "Benchmark on Deterministic Transport Calculation with Spatial Homogenization," OECD/NEA Report, NEA/NSC/DOC(2003)16, (2003).
7) B. C. Na, "Benchmark on the Three-Dimensional VENUS-2 MOX Core Measurements," OECD/NEA Report, NEA/NSC/DOC (2003).
8) Z. Zhong, T. J. Downar, H. G. Joo, and J. Y. Cho, "Benchmark Analysis of the DeCART MOC Code with the VENUS-2 Critical Experiment," Proc. PHYSOR2004 – The Physics of Fuel Cycles and Advanced Nuclear Systems: Global Developments, Chicago, Illinois, April 25-29, CD-ROM, American Nuclear Society, Lagrange Park, IL. (2004).
9) H. J. Shim, B. S. Han, and C. H. Kim, "Numerical Experiment on Variance Biases and Monte Carlo Neutronics Analysis with Thermal Hydraulic Feedback," International Conference on Supercomputing in Nuclear Application, SNA03, Paris, France, Sept. 22-24, 2003, Paper 103, CD-ROM (2003).
10) H. G. Joo, et al., "Consistent Comparison of Monte Carlo and Whole-Core Transport Solutions for Cores with Thermal Feedback," Proc. PHYSOR2004 – The Physics of Fuel Cycles and Advanced Nuclear Systems: Global Developments, Chicago, Illinois, April 25-29, on CD-ROM, American Nuclear Society, Lagrange Park, IL. (2004).
11) H. G. Joo, et al., "Effectiveness of the Whole Core Transport Calculation with Pin-Wise Thermal Feedback" Advances in Nuclear Fuel Management III (ANFM 2003) Hilton Head Island, South Carolina, USA, October 5-8, 2003, CD-ROM, American Nuclear Society, LaGrange Park, IL (2003).
12) B. O. Cho et al., "MASTER-2.0: Multi-purpose Analyzer for Static and Transient Effects of Reactors," KAERI/TR-1211/99, Korea Atomic Energy Research Institute, Jan. 1999 (1999).
13) J. Y. Cho, at al., "Parallelization of Three-Dimensional Whole Core Transport Code DeCART," International Conference on Supercomputing in Nuclear Application, SNA03, Paris, France, Sept. 22-24, 2003, Paper 62, CD-ROM (2003).
14) J. Y. Cho, H. G. Joo, K. S. Kim, and S. Q. Zee, "Cell-Based CMFD Formulation for Acceleration of Whole-core Method of Characteristics Calculations," *J. Kor Nucl Soc.*, **35**, *pp.* 250-258 (2002).
15) J. Y. Cho, et al., "Three-Dimensional Whole Core Transport Calculation Methodology of the DeCART Code," KAERI Report TR-2365/2003 (2003).
16) H. G. Joo and T. J. Downar. "An Incomplete Domain Decomposition Preconditioning Method for Nonlinear Nodal Kinetics Calculation," *Nucl. Sci. Eng.*, **123,** *pp*.403-414 (1996).